

Anisotropic surface effects on the formation of chiral morphologies of nanomaterials

Jian-Shan Wang, Hai-Mu Ye, Qing-Hua Qin, Jun Xu and Xi-Qiao Feng

Proc. R. Soc. A 2012 **468**, 609-633 first published online 26 October 2011
doi: 10.1098/rspa.2011.0451

References

This article cites 56 articles, 6 of which can be accessed free

<http://rspa.royalsocietypublishing.org/content/468/2139/609.full.html#ref-list-1>

Subject collections

Articles on similar topics can be found in the following collections

[mechanics](#) (73 articles)

[nanotechnology](#) (30 articles)

Email alerting service

Receive free email alerts when new articles cite this article - sign up in the box at the top right-hand corner of the article or click [here](#)

Anisotropic surface effects on the formation of chiral morphologies of nanomaterials

BY JIAN-SHAN WANG^{1,2,*}, HAI-MU YE³, QING-HUA QIN⁴, JUN XU³
AND XI-QIAO FENG^{2,*}

¹*Department of Mechanics and Tianjin Key Laboratory of Modern Engineering Mechanics, Tianjin University, Tianjin 300072, People's Republic of China*

²*AML and CNMM, Department of Engineering Mechanics, and*

³*Institute of Polymer Science and Engineering, Department of Chemical Engineering, School of Materials Science and Technology, Tsinghua University, Beijing 100084, People's Republic of China*

⁴*Research School of Engineering, Australian National University, Canberra, Australian Capital Territory 0200, Australia*

Nanomaterials with chiral morphologies hold promise for a wide diversity of technologically important applications in such fields as micro/nano-electromechanical systems and medical engineering. Understanding the mechanisms underlying the formation of chiral morphologies of natural and synthesized materials remains an issue of crucial significance. In this study, a refined Kirchhoff rod model taking into account anisotropic surface effects is employed to describe quasi-one-dimensional nanomaterials with complicated spatial morphologies. It is shown that anisotropic surface stresses can induce the formation of rich morphologies of nanomaterials. A general shape equation of nanowires is derived by the variational method of energy. Thereby, the effects of anisotropic surface properties, bulk elastic properties and cross-sectional sizes on the chiral morphologies of nanomaterials are quantitatively investigated, and the conditions for the formation of binormal nanohelices are given. The physical mechanism addressed in this study is verified by our recent experiments on tuning the twisting chirality of polymer lamellae via surface treatments. Our analysis suggests that one can design and adjust the morphology of synthesized nanohelices by tailoring or functionalizing their surfaces during fabrication. This study is also helpful in interpreting the formation of such artificial and biological chiral materials as the flagella of bacterial and self-assembled helical ribbons.

Keywords: nanomaterials; nanohelix; size effect; chiral morphology; anisotropic surface stress

1. Introduction

Quasi-one-dimensional nanomaterials such as nanotubes, nanowires and nanobelts have attracted the attention, imagination and close scrutiny of

*Authors for correspondence (wangjs@tju.edu.cn; fengqx@tsinghua.edu.cn).

scientists and engineers over the past decade. This scrutiny derives from their promising applications in a broad range of industrial fields. They have been used, for instance, as sensors, actuators, transducers and other building blocks for various micro/nanodevices and systems. Some 'bottom-up' and 'top-down' techniques have been developed to produce nanowires and nanobelts made of metals, semiconductors, oxides and polymers. Interestingly, these quasi-one-dimensional nanomaterials may assume different morphologies (e.g. straight, kinked, wavy, twisted and helical shapes), which can be further assembled into more complex structures.

Chiral shapes are widely observed in synthesized materials and biological and self-assembled organic systems. Some typical examples are ZnO and SiO_x nanobelts of helical shape (Kong & Wang 2003; Gao *et al.* 2005; Kim & Shim 2007), amorphous boron carbide nanosprings (McIlroy *et al.* 2001), twisting carbon nanoribbons (Chen *et al.* 2005), twisting polymer lamellae (Lotz & Cheng 2005), self-assembled helical ribbons (Zastavker *et al.* 1999; Smith *et al.* 2001), the capsids of viruses and the flagella of bacteria (e.g. *Salmonella* and *Escherichia coli*; Cahill 2005; Kim & Powers 2005). Although nanowires are required to have a straight shape for applications in certain fields, the helical morphology of nanobelts or nanoribbons of such materials as ZnO endows the materials with some unusual properties, e.g. superior elastic properties. Spiral micro/nanomaterials, including nanosprings, nanocoils and helical nanobelts, have found diverse novel applications as, for instance, sensors and probes in biomedical and nanoengineering areas (Zastavker *et al.* 1999; Smith *et al.* 2001; Chen *et al.* 2005; Gao *et al.* 2005; Korgel 2005; Kim & Shim 2007). For example, nanohelices can be used to measure the forces and energies associated with interacting biological macromolecules and to quantitatively characterize the elastic properties of biological structures such as one-dimensional chains and two-dimensional membranes (Zastavker *et al.* 1999).

Although many biological and synthesized nanohelices assume helical or twisting morphologies in a wide range of size scales, the origins of the formation of such asymmetric shapes remain unclear in many cases. Much effort has been directed towards exploring the formation mechanisms of the helical double structure of DNA and the twisted shape of polymer lamellae. Snir & Kamien (2005) proposed a heuristic, entropically based model for a system of hard spheres and semiflexible tubes to explain the helical conformations of biopolymers. By analysing the regular assembly of identical objects, Cahill (2005) theoretically illustrated that biological structures such as DNA, protein and virus capsids prefer helical geometry. Investigation of the twisting mechanisms of polymer lamellae remains a challenging issue in the field of polymer science, although some possible mechanisms at the molecular or grain level have been proposed, including the asymmetric supply of material to the growth front of polymer lamellae, nucleation of screw dislocations in growing lamellae and surface stresses associated with chain folding (Lotz & Cheng 2005). Zastavker *et al.* (1999) examined the self-assembly of helical crystalline ribbons in a variety of multi-component enantiomerically pure systems. They found that, in almost all systems, two distinctly different pitch lengths of helical ribbons could be formed, and both right- and left-handed chiralities were observable. Therefore, they concluded that molecular chirality is not the determining factor in helix

formation. Recently, Khaykovich *et al.* (2007) further examined the structure of cholesterol helical ribbons and self-assembled biological springs at the molecular and granular levels.

Another important issue is the control and optimization of the morphology and growth processes of chiral nanomaterials. In contrast to the formation of straight nanowires, the synthesis of helical nanostructures is often more complex and requires either the existence of anisotropic growth or asymmetric forces at a certain level (Fonseca *et al.* 2007). Considering a vapour–liquid–solid growth mechanism, McIlroy *et al.* (2001) developed a contact angle anisotropy model to demonstrate that anisotropic contact between the catalyst and the nanowire can lead to the formation of amorphous helical nanostructures. Subsequently, they attributed the formation of biphase (crystalline core/amorphous sheath) helical nanowires to the different growth rates of the two phases induced by the existence of temperature gradients within the catalyst (Zhang *et al.* 2003). More recently, Fonseca *et al.* (2007) studied the effect of catalyst shape on the cross-sectional shape of nanosprings and discussed the possibility of growth of normal and binormal nanosprings. In addition, Amelinckx *et al.* (1994) proposed a spatial velocity hodograph-based model to interpret the helical growth of carbon nanotubes, and Bandaru *et al.* (2007) addressed the formation mechanisms of helical nanotube/fibres from the viewpoint of thermodynamics.

In spite of these previous developments, however, there is still a lack of quantitative investigations on the mechanisms underlying the formation of chiral morphology of micro/nanosized materials. Nanomaterials have a large ratio between surface area and volume, and their atoms near surfaces experience a local environment distinct from those in the bulk. Therefore, surface stress and surface energy often have a substantial influence on the growth, material properties and physical behaviours of nanosized materials and devices (Dingreville *et al.* 2005; Park & Klein 2008; Zhang *et al.* 2008; Ru 2010). To account for the effect of surface stress and surface energy, Gurtin & Murdoch (1975) and Gurtin *et al.* (1995) presented a continuum mechanics theory by treating the surface as a two-dimensional coherent membrane adhering to the bulk. This surface elasticity theory has been adopted to study the static and dynamic deformation behaviours of nanosized structure elements such as plates, beams and bars, and the results agree well with those from atomic simulations (Miller & Shenoy 2000; Shenoy 2002). Therefore, the theory provides an efficient tool for understanding various size-dependent phenomena at the micro- and nanoscales (Sharma *et al.* 2003; He *et al.* 2004; Duan *et al.* 2005; Lu *et al.* 2006; Tian & Rajapakse 2007; Wang, G. F. *et al.* 2007; Wang, J. S. *et al.* 2010; Wang, Z. J. *et al.* 2010; Huang & Kang 2011; Xia *et al.* 2011).

It has been recognized that surface stresses play an important role in surface reconstruction, diffusion, growth and evolution of nanomaterials (Lu & Suo 2002; Siegel *et al.* 2004). However, the effects of surface stresses on the morphology of nanowires have been little addressed. For most metallic, semiconducting and even polymeric materials, surfaces/interfaces have anisotropic properties, which often induce orientation-dependent surface stresses. For example, the interface stresses on the {201} polyethylene crystal surface are anisotropic, with the values of approximately -0.27 and -0.4 J m^{-2} along the two main directions of the interface, respectively (Hütter *et al.* 2006). Anisotropic surface stresses on W(110) and Ge(001) were reported by Sander *et al.* (1999) and Middel *et al.* (2002),

respectively. In addition, different surfaces of a material often have different properties for such reasons as synthesis process, chain folding and constraint conditions. Recently, Wang *et al.* (2008) and Ye *et al.* (2010) demonstrated, through theoretical analysis and experiments, that anisotropic surface stresses can induce the twisting of nanobelts and polymer lamellae, which is only a special case of three-dimensional chiral morphologies. However, how the anisotropic surface stresses affect the formation of general chiral morphologies of nanomaterials such as nanohelices remains elusive.

In this study, we investigate the effects of anisotropic surface stresses on the formation of chiral morphologies of quasi-one-dimensional nanomaterials. The refined Kirchhoff rod model with isotropic surface effects (Wang, J. S. *et al.* 2010) is first generalized to the case of anisotropic surface effects. Using this model, a general shape equation that controls the spatial equilibrium morphology of nanowires is derived and, thereby, the necessary conditions for the formation of binormal nanohelices are given. Effects of the elastic properties of surface and bulk materials are examined on the chiral morphologies of nanohelices. The theoretical results are validated by our recent experiments (Ye *et al.* 2010).

2. Refined Kirchhoff rod model with anisotropic surface effects

(a) Kirchhoff rod model

The Kirchhoff rod model provides an efficient theoretical tool to study the static and dynamic behaviour of long rods, which may undergo large change of shape. It has been used to model the deformation behaviour of long DNA chains, the tendrils of climbing plants, ropes and cables, etc. (Fonseca & Galvão 2004; Goriely & Neukirch 2006; Liu 2006). Recently, the effect of surface stresses has been implemented into the Kirchhoff rod model using the concept of surface elasticity (Wang, J. S. *et al.* 2010). In the present study, this model is extended to describe the spatial morphology of quasi-one-dimensional nanomaterials associated with anisotropic surface effects.

Consider a slender nanowire such as a nanobelt or a nanolamella of length l , as shown in figure 1. For illustration, it is assumed to have a rectangular cross section of width b and thickness h , with $l \gg b \gg h$, although other cross-sectional shapes can be analysed similarly. Here, the nanowire is treated as a Kirchhoff rod with anisotropic properties of the surface elasticity. We describe the spatial geometry of the morphology of a curved Kirchhoff rod in terms of both the principal axes-based Cartesian coordinate system (o - xyz) and the local Frenet coordinate system (o - NBT), as shown in figure 2a, where the origin o is located on the centreline. The x and y axes are along the principal axes of the cross section of the nanowire, the z and T axes are along the tangent direction of the centreline, and the N and B axes are along the normal and binormal vectors of the centreline, respectively. The unit vectors along the T , N and B axes are denoted as \mathbf{n} , \mathbf{b} and \mathbf{t} , respectively. Let χ designate the angle measured from the x -axis to the N -axis.

With reference to the two coordinate systems, we can describe not only the spatial geometry change of the centreline of the deformable nanowire but also the relative rotation of its cross section with respect to the centreline. The

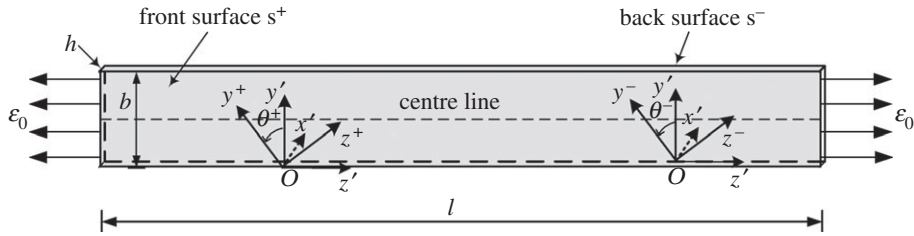


Figure 1. An originally straight nanobelt, whose front and back surfaces have different anisotropic elastic properties.

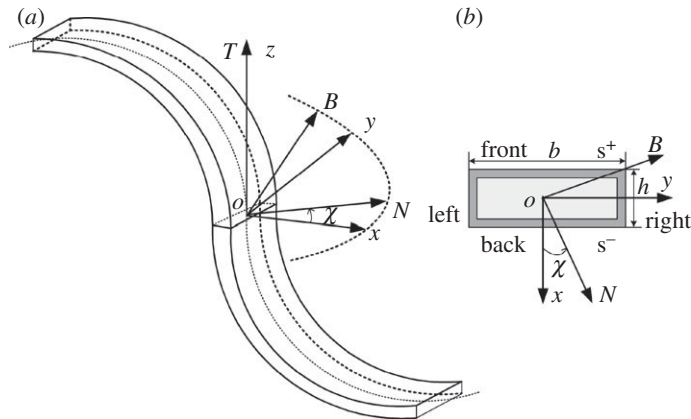


Figure 2. (a) The principal axes of the cross section ($o-xyz$) and the Frenet coordinate system ($o-NBT$) in a thin and long nanobelt. (b) Its cross section and surface layer.

twisting of the nanowire can be characterized by a twisting vector $\boldsymbol{\omega}$, which is expressed as

$$\omega_1 = \kappa \sin \chi, \quad \omega_2 = \kappa \cos \chi \quad \text{and} \quad \omega_3 = \tau + \frac{d\chi}{ds}, \quad (2.1)$$

where ω_i ($i=1, 2, 3$) denote the components of $\boldsymbol{\omega}$ in the x , y and z directions, respectively, and κ denotes the curvature of the centreline at point o and τ is the torsion of the nanowire (Liu 2006). For a nanowire with a rectangular cross-section as shown in figure 2b, the two principal moments of inertia along the principal axes are $I_x = (1/12)hb^3$ and $I_y = (1/12)h^3b$. A helical morphology will be referred to as normal or binormal (Fonseca *et al.* 2007), if the direction of its greatest bending stiffness is along the unit vector \mathbf{n} or \mathbf{b} , respectively, as shown in figure 3a,b. In the following, the existence of both binormal and normal helical nanowires will be discussed.

According to the Kirchhoff rod model, the stresses and strains in the bulk of the nanowire with a long and narrow rectangular cross section ($b \gg h$) can be expressed as (Wang, J. S. *et al.* 2010)

$$\sigma_3 = E(\omega_1 y - \omega_2 x), \quad \tau_{23} = \tau_{32} = 2G\omega_3 x, \quad (2.2)$$

and

$$\varepsilon_3 = \omega_1 y - \omega_2 x, \quad \varepsilon_{23} = \varepsilon_{32} = \omega_3 x, \quad (2.3)$$

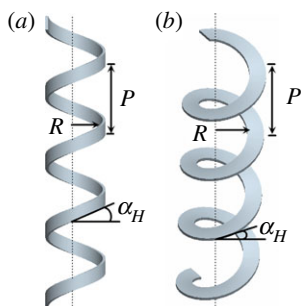


Figure 3. (a) Binormal and (b) normal helical nanobelts. (Online version in colour.)

where E and G are Young's modulus and the shear modulus of the bulk material, respectively.

(b) Surface elasticity

The front and the back surfaces of the nanowire are denoted by s^+ and s^- , respectively, as shown in figures 1 and 2b. The two surfaces may have different elastic properties for such reasons as different surface structures, growth processes and chain-folding manners (Lotz & Cheng 2005). For the sake of simplicity, we assume that the two surfaces have different anisotropic elastic properties and their main elastic axes have different orientations. Refer to the global Cartesian coordinate system ($o-xyz$) in figure 1, where the y and z axes are along the width and length directions, respectively. In the case of small strains, it is reasonable to assume that the surface constitutive relations are linearly elastic and orthotropic. The main axes of the constitutive relation on the initial front surface s^+ are along the y^+ and z^+ axes, with an angle θ^+ measured from z to z^+ , whereas the main axes on the back surface s^- are along the y^- and z^- axes, with an angle θ^- measured from z to z^- . Here and in the following, the superscripts '+' and '-' stand for the parameters on the initial front and back surfaces, respectively.

The surface elastic constitutive relations in the coordinate system ($o-x^+y^+z^+$) or ($o-x^-y^-z^-$) can be written as (Gurtin & Murdoch 1975)

$$\sigma_{\alpha\beta}^s = \tau_{\alpha\beta}^0 + c_{\alpha\beta\gamma\delta}^s \varepsilon_{\gamma\delta}^s, \quad (2.4)$$

where $\sigma_{\alpha\beta}^s$ denote the surface stresses, $\varepsilon_{\gamma\delta}^s$ the surface strains, $\tau_{\alpha\beta}^0$ the residual surface stress or surface eigenstress (Zhang *et al.* 2010) and $c_{\alpha\beta\gamma\delta}^s$ the surface elastic constants. Throughout this study, Einstein's summation convention is adopted for all repeated Latin indices over (1, 2, 3) and Greek indices over (1, 2).

The surface elastic properties in the global coordinate system ($o-xyz$) can be obtained by coordinate transformation as (Wang *et al.* 2008)

$$\left. \begin{aligned} \sigma_{yy}^{\pm} &= c_{11}^{\pm} \varepsilon_{yy}^{\pm} + c_{12}^{\pm} \varepsilon_{zz}^{\pm} + c_{13}^{\pm} \varepsilon_{zy}^{\pm}, \\ \sigma_{zz}^{\pm} &= \tau_0^{\pm} + c_{21}^{\pm} \varepsilon_{xx}^{\pm} + c_{22}^{\pm} \varepsilon_{zz}^{\pm} + c_{23}^{\pm} \varepsilon_{zy}^{\pm}, \\ \tau_{zy}^{\pm} &= c_{31}^{\pm} \varepsilon_{yy}^{\pm} + c_{32}^{\pm} \varepsilon_{zz}^{\pm} + c_{33}^{\pm} \varepsilon_{zy}^{\pm}, \end{aligned} \right\} \quad (2.5)$$

and

where τ_0^\pm is the axial residual surface stresses, and c_{ij}^\pm denote the surface elastic coefficients on the two surfaces, respectively. For example, c_{ij}^+ can be expressed as

$$\left. \begin{aligned} c_{11}^+ &= c_{1111}^{s+} \cos^4 \theta^+ + 2(c_{1122}^{s+} + 2c_{1212}^{s+}) \cos^2 \theta^+ \sin^2 \theta^+ + c_{2222}^{s+} \sin^4 \theta^+, \\ c_{12}^+ &= (c_{1111}^{s+} + c_{2222}^{s+} - 4c_{1212}^{s+}) \cos^2 \theta^+ \sin^2 \theta^+ + c_{1212}^{s+} (\cos^4 \theta^+ + \sin^4 \theta^+), \\ c_{22}^+ &= c_{1111}^{s+} \sin^4 \theta^+ + 2(c_{1122}^{s+} + 2c_{1212}^{s+}) \cos^2 \theta^+ \sin^2 \theta^+ + c_{2222}^{s+} \cos^4 \theta^+, \\ c_{31}^+ &= (-c_{1111}^{s+} + c_{1122}^{s+} + 2c_{1212}^{s+}) \cos^3 \theta^+ \sin \theta^+ \\ &\quad + (-c_{1122}^{s+} + c_{2222}^{s+} - 2c_{1212}^{s+}) \cos \theta^+ \sin^3 \theta^+, \\ c_{32}^+ &= (-c_{1111}^{s+} + c_{1122}^{s+} + 2c_{1212}^{s+}) \cos \theta^+ \sin^3 \theta^+ \\ &\quad + (-c_{1122}^{s+} + c_{2222}^{s+} - 2c_{1212}^{s+}) \cos^3 \theta^+ \sin \theta^+, \\ c_{33}^+ &= \frac{1}{2}(c_{1111}^{s+} + c_{2222}^{s+} - 2c_{1212}^{s+}) \sin^2 2\theta^+ + 2c_{1212}^{s+} \cos^2 2\theta^+, \\ c_{13}^+ &= 2c_{31}^+ \quad \text{and} \quad c_{23}^+ = 2c_{32}^+. \end{aligned} \right\} \quad (2.6)$$

During the formation of a helical nanowire, the curvature radius is assumed to be much larger than the sizes of the cross section, i.e. $|kb| \ll 1$. According to the surface elasticity theory, the front and back surfaces of the nanowire are considered to adhere perfectly to the bulk without slipping being allowed, and the equilibrium equations on the surfaces are written as (Gurtin & Murdoch 1975; Gurtin *et al.* 1995)

$$\sigma_{\xi\eta,\xi}^\pm - \sigma_{\eta j} n_j = 0 \quad \text{and} \quad \sigma_{ij} n_i n_j = \sigma_{\xi\eta}^\pm \kappa_{\xi\eta}^\pm, \quad (2.7)$$

where σ_{ij} are the stresses in the bulk material, $\sigma_{\xi\eta}^\pm$ are the surface stresses and n_i is the unit normal vector of the surface.

It should be noted that surface properties are generally defined as the excess over the values of the bulk properties (Gibbs 1928). Surface structures of some nanomaterials such as polymer lamellae can be changed by surface treatments and the oriented chain-folding of polymer macromolecules, which can render anisotropic surface properties. In such cases, the anisotropic surface with an isotropic bulk material can still be described with the concepts of *dividing surfaces* and *excess quantities* defined by Gibbs (1928). Furthermore, the model we present in this study is also applicable to nanowires with an anisotropic core.

(c) Equilibrium equations

For a nanowire with a rectangular cross section ($b \gg h$), equation (2.7) indicates that the surface stresses induce an effective distributed transverse force on the centreline, f_1 , along the x direction. f_1 can be obtained as

$$f_1 = (\tau_0^+ + \tau_0^-) b \omega_2 + \frac{1}{2}(c_{22}^+ - c_{22}^-) b h \omega_2^2 - (c_{32}^+ - c_{32}^-) b h \omega_2 \omega_3. \quad (2.8)$$

Because $h \ll b \ll l$, the effect of surface stresses on the left and right surfaces can be neglected, i.e. $f_2 = 0$. Similarly, $f_3 = 0$ and $m_1 = m_3 \approx 0$. A distributed moment m_2 in the y direction is also induced by the residual surface stresses. m_2 is given as

$$m_2 = \frac{1}{2}(\tau_0^+ - \tau_0^-)bh. \quad (2.9)$$

Then, the modified Kirchhoff equations to describe the equilibrium of the nanowire with $b \gg h$ in the principal axes-based Cartesian coordinate system ($o - xyz$) read

$$\frac{d\mathbf{F}}{ds} + \boldsymbol{\omega} \times \mathbf{F} + \mathbf{f} = 0 \quad (2.10)$$

and
$$\frac{d\mathbf{M}}{ds} + \boldsymbol{\omega} \times \mathbf{M} + \mathbf{e}_3 \times \mathbf{F} + \mathbf{m} = 0, \quad (2.11)$$

where \mathbf{F} and \mathbf{M} are the internal force and moment on the cross section, respectively. \mathbf{M} can be obtained by

$$M_1 = A_1^* \omega_1, \quad M_2 = B_1^* \omega_2 + B_2^* \omega_3 \quad \text{and} \quad M_3 = C_1^* \omega_3 + C_2^* \omega_2, \quad (2.12)$$

where

$$\left. \begin{aligned} A_1^* &= \frac{1}{12} [Eh^3 + (c_{22}^+ + c_{22}^-)b^2] b, \\ B_1^* &= \frac{1}{12} [Eh + 3(c_{22}^+ + c_{22}^-)] bh^2, \quad B_2^* = -\frac{1}{2}(c_{32}^+ + c_{32}^-)bh^2 \\ \text{and} \quad C_1^* &= \frac{1}{6} [2Gh + 3(c_{33}^+ + c_{33}^-)] bh^2, \quad C_2^* = -\frac{1}{2}(c_{32}^+ + c_{32}^-)bh^2. \end{aligned} \right\} \quad (2.13)$$

The force \mathbf{f} and the moment \mathbf{m} induced by the residual surface stresses are given by

$$\mathbf{f} = f_1 \mathbf{e}_1 + f_2 \mathbf{e}_2 + f_3 \mathbf{e}_3 \quad \text{and} \quad \mathbf{m} = m_1 \mathbf{e}_1 + m_2 \mathbf{e}_2 + m_3 \mathbf{e}_3, \quad (2.14)$$

where $f_2 = f_3 = 0$ and $m_1 = m_3 = 0$.

Submitting equations (2.12)–(2.14) into (2.10), the Kirchhoff equations can be formulated in terms of the components of the force \mathbf{f} and the moment \mathbf{m} . The equilibrium condition of the moments in the z direction requires that

$$\frac{dM_3}{ds} + \omega_1 M_2 - \omega_2 M_1 = 0. \quad (2.15)$$

Using equations (2.1) and (2.11), equation (2.15) can become

$$C_1^* \frac{d\omega_3}{ds} + B_2^* \kappa \omega_3 \sin \chi = (A_1^* - B_1^*) \kappa^2 \sin \chi \cos \chi + C_2^* \kappa \frac{d(\cos \chi)}{ds}. \quad (2.16)$$

As in the classical Kirchhoff problem for a helical rod, equations (2.10) and (2.11) for a nanowire have solutions corresponding to chiral morphologies like twisting nanobelts and nanohelices. For a rectangular cross-sectional nanowire ($A_1^* \neq B_1^*$) with a chiral morphology, ω_3 has a constant value. From equation (2.16), we obtain the following special solution corresponding to a regular three-dimensional chiral morphology with a constant twist:

$$\chi = n\pi \quad (n = 0, 1, 2, \dots). \quad (2.17)$$

Without loss of generality, let $\chi = 0$, that is, the principal axes-based Cartesian coordinate system ($o - xyz$) coincides with the local Frenet coordinate system ($o - NBT$). In this case, one has

$$\omega_1 = 0, \quad \omega_2 = \kappa_0 \quad \text{and} \quad \omega_3 = \tau_0, \quad (2.18)$$

where κ_0 and τ_0 are constants. Equation (2.18) indicates that the nanowire assumes the shape of a binormal nanohelix. For the normal nanohelices, $\chi = \pi/2$, which cannot satisfy equation (2.16). Thus, anisotropic surface effects will not induce a normal helical morphology.

Another special solution of equation (2.16) is

$$\kappa = 0, \quad \tau = 0 \quad \text{and} \quad \chi = \tau^* s, \quad (2.19)$$

where τ^* , the twist angle per unit length, is a constant and s is the arc length. In this case, the nanowire has the shape of a twisting nanobelt. Other solutions of equation (2.16) correspond to more complicated spatial morphologies with non-uniform curvature and torsion.

3. Two typical chiral morphologies of nanomaterials

Owing to factors such as temperature change, concentration gradient and chain folding during the synthesis or fabrication process, residual strains and stresses often arise in metal, semiconductor or polymer nanowires. As a consequence of anisotropic surface elasticity, the nanowire will bend and twist simultaneously into different spatial shapes, rendering partial release of residual strains–stresses. In addition, the anisotropic surface eigen displacements induced by surface energy relaxation (Zhang *et al.* 2011) can also deform nanowires into different morphologies and may serve as another driving force for the formation of chiral materials.

In principle, the above-refined Kirchhoff rod model allows us to analyse the deformation of quasi-one-dimensional materials of arbitrary geometry with surface effects. In this section, we will consider, for simplicity, the two most representative chiral morphologies, i.e. twisting nanobelts and binormal nanohelices, which are widely observed in experiments and are of particular interest for applications. The mechanism of anisotropic surface stresses underlying the formation of chiral morphologies of nanomaterials will also be verified by comparing with relevant experiments.

(a) Twisting nanobelts

Experimental observations found that some quasi-one-dimensional nanomaterials have a twisting shape, and the theoretical analysis of Wang *et al.* (2008) showed that the formation of such an asymmetric shape may originate from the effect of anisotropic surface stresses. For completeness and comparison, we briefly summarize the solution of a twisting nanobelt. For a nanobelt of length l , width b and thickness h , the potential energy is expressed as

$$\begin{aligned} \Pi = & \frac{1}{2} E \varepsilon^2 b h l + \frac{1}{6} G \tau'^2 b h^3 l + (\tau_0^+ + \tau_0^-) \varepsilon b l + \frac{1}{2} (c_{22}^+ + c_{22}^-) \varepsilon^2 b l \\ & + (c_{32}^+ - c_{32}^-) \tau' \varepsilon b h l + \frac{1}{4} (c_{33}^+ + c_{33}^-) \tau'^2 b h^2 l - F \varepsilon l, \end{aligned} \quad (3.1)$$

where F is the force associated with the growth process, ε the axial strain component and τ' the twist angle per unit length. It should be mentioned that, besides the force F , some other factors, e.g. the change of temperature and concentration gradient, can also deform nanowires and can be analysed similarly.

Using the variational principle of energy with respect to ε and τ' , one obtains (Wang *et al.* 2008)

$$D_1\varepsilon + D_2\tau' = \sigma_0, \quad \varepsilon = D_3\tau', \quad (3.2)$$

with

$$\left. \begin{aligned} D_1 &= E + \frac{1}{h}(c_{22}^+ + c_{22}^-), & D_2 &= c_{32}^- - c_{32}^+ \\ D_3 &= \frac{2Gh^2 + 3(c_{22}^+ + c_{22}^-)h}{6(c_{32}^+ - c_{32}^-)}, & \sigma_0 &= \frac{F}{bh} - \frac{1}{h}(\tau_0^+ + \tau_0^-). \end{aligned} \right\} \quad (3.3)$$

and

The half-twisting pitch length can be derived as

$$L(h) = \frac{\pi}{\tau'} = \frac{\pi}{\sigma_0}(D_1D_3 + D_2). \quad (3.4)$$

Evidently, the half-twisting pitch length depends on the elastic properties of the surfaces and the bulk material as well as the geometry of the cross section.

(b) Binormal nanohelices

In the second representative example, we assume that the axial residual strain component in the originally straight state of the nanowire is ε_0 . In addition, the nanowire may have an initial twisting τ_0^* induced by growth. For a slender nanowire of a rectangular cross section with $l \gg b \gg h$, the normal stress component σ_{yy} along its thickness direction is generally negligible. We take the initial state of the nanowire with the axial residual strain and the initial twisting as the reference configuration. Its potential energy is

$$\Pi^i = (H_{\text{bulk}}^i + H_{\text{sur}}^i)l, \quad (3.5)$$

where H_{bulk}^i and H_{sur}^i denote the energies in the bulk and on the surfaces, respectively. They are expressed as

$$H_{\text{bulk}}^i = \frac{1}{2}Ebh\varepsilon_0^2 + \frac{1}{6}Gbh^3\tau_0^{*2} \quad (3.6)$$

$$\begin{aligned} \text{and} \quad H_{\text{sur}}^i &= (\tau_0^+ + \tau_0^-)b\varepsilon_0 + \frac{1}{2}(c_{22}^+ + c_{22}^-)b\varepsilon_0^2 + \frac{3}{2}(c_{32}^+ - c_{32}^-)bh\tau_0^*\varepsilon_0 \\ &\quad + \frac{1}{8}(c_{33}^+ + c_{33}^-)bh^2\tau_0^{*2}, \end{aligned} \quad (3.7)$$

where the superscript 'i' stands for the quantities in the initial or reference configuration.

After the release of the axial residual strain and the initial twisting, the nanowire will have a spatial shape with curvature $\kappa(s)$ and torsion $\tau(s)$, which are functions of the arc length s . For simplicity, it is assumed that the nanowire has no self-twisting, i.e. $\chi = 0$. In the current configuration, the centreline of the nanowire with bending and twisting deformations will be a spatial curve. According to

equation (2.3), the surface strain components in the deformed nanowire can be expressed as

$$\varepsilon_{zz}^{c+} = \frac{1}{2}h\kappa(s), \quad \varepsilon_{zy}^{c+} = -\frac{1}{2}h\tau(s), \quad \varepsilon_{zz}^{c-} = -\frac{1}{2}h\kappa(s) \quad \text{and} \quad \varepsilon_{zy}^{c-} = \frac{1}{2}h\tau(s), \quad (3.8)$$

where the superscript ‘c’ indicates the quantities in the current configuration.

Using equations (2.5) and (3.8), the potential energy of nanowires in the current configuration is derived as

$$\Pi^c = \int (H_{\text{bulk}}^c + H_{\text{surf}}^c) ds, \quad (3.9)$$

where

$$H_{\text{bulk}}^c = \frac{1}{2}B_1\kappa(s)^2 + \frac{1}{2}C_1\tau(s)^2 \quad (3.10)$$

$$\text{and } H_{\text{surf}}^c = \frac{1}{2}(\tau_0^+ - \tau_0^-)bh\kappa(s) + \frac{1}{8}(c_{22}^+ + c_{22}^-)bh^2\kappa(s)^2 - \frac{3}{4}(c_{32}^+ + c_{32}^-)bh^2\kappa(s)\tau(s) \\ + \frac{1}{8}(c_{33}^+ + c_{33}^-)bh^2\tau(s)^2, \quad (3.11)$$

with $B_1 = \frac{1}{12}Eh^3b$ being the bending stiffness of the nanowire with respect to the y -axis and $C_1 = \frac{1}{3}Gbh^3$ being the torsion rigidity.

From equations (3.5) and (3.9), the change in the potential energy from the reference state to the current state is

$$\Pi = \Pi^c - \Pi^i = \int H_0 ds, \quad (3.12)$$

where

$$H_0 = \frac{1}{2}[-Q_0 + Q_1\kappa(s) + Q_2\kappa^2(s) + Q_3\kappa(s)\tau(s) + Q_4\tau^2(s)], \quad (3.13)$$

$$\left. \begin{aligned} Q_0 &= (Eh + c_{22}^+ + c_{22}^-)b\varepsilon_0^2 + \frac{1}{4}[4C_1 + (c_{33}^+ + c_{33}^-)bh]\tau_0^{*2} + 2(\tau_0^+ + \tau_0^-)b\varepsilon_0 \\ &\quad + \frac{3}{4}(c_{32}^+ - c_{32}^-)bh\tau_0^*\varepsilon_0, \\ Q_1 &= (\tau_0^+ - \tau_0^-)bh, \quad Q_2 = \frac{1}{4}[4B_1 + (c_{22}^+ + c_{22}^-)bh^2], \\ Q_3 &= -\frac{3}{2}(c_{32}^+ + c_{32}^-)bh^2 \quad \text{and} \quad Q_4 = \frac{1}{4}[4C_1 + (c_{33}^+ + c_{33}^-)bh^2]. \end{aligned} \right\} \quad (3.14)$$

The equilibrium and stability of a nanowire require

$$\Pi \leq 0, \quad \delta\Pi = 0 \quad \text{and} \quad \delta^2\Pi \geq 0, \quad (3.15)$$

where

$$\delta\Pi = \int \frac{\partial H_0}{\partial \kappa} \delta\kappa ds + \int \frac{\partial H_0}{\partial \tau} \delta\tau ds + \int H_0 \delta ds. \quad (3.16)$$

The centreline of a nanowire $\mathbf{r} = \mathbf{r}(s)$ can be described in terms of the orthonormal Frenet basis $\{\mathbf{r}(s); \mathbf{e}_1(s), \mathbf{e}_2(s), \mathbf{e}_3(s)\}$, where $\mathbf{e}_1(s)$ is the unit tangent vector, $\mathbf{e}_2(s)$ is the unit normal vector and $\mathbf{e}_3(s)$ is the unit binormal vector of the centreline of the nanowire.

The Frenet equations are

$$d\mathbf{e}_i = w_{ij}\mathbf{e}_j, \quad w_{ij} + w_{ji} = 0, \quad (3.17)$$

where

$$w_{1,2} = -w_{2,1} = \kappa(s)ds, \quad w_{2,3} = -w_{3,2} = \tau(s)ds. \quad (3.18)$$

Using the calculus of variations (Ou-Yang & Su 1997; Tu *et al.* 2006; Zhao *et al.* 2006; Gao *et al.* 2008), we can derive the expression of $\delta\Pi$. It should be mentioned that, owing to the inextensibility assumption of the bent and twisted nanowire, the variation $\delta\Pi$ depends only on the variation of the centreline of the nanowire along the normal (\mathbf{e}_2) and binormal (\mathbf{e}_3) directions. Using $\delta\mathbf{r} = \Omega_2\mathbf{e}_2$ and $\delta\mathbf{e}_i = \Omega_{ij}\mathbf{e}_j$, in conjunction with the relation (Tu *et al.* 2006)

$$\left. \begin{aligned} \delta ds &= \Omega_2 w_{21} = -\kappa ds \Omega_2, & \Omega_{23} ds &= \frac{1}{\kappa} [2d(\tau\Omega_2) - \Omega_2 d\tau], \\ \delta\kappa ds &= d\Omega_{12} + (\kappa^2 - \tau^2)\Omega_2 ds & \text{and} & \quad \delta\tau ds = d\Omega_{23} + 2\kappa\tau d\Omega_2, \end{aligned} \right\} \quad (3.19)$$

we obtain

$$\left. \begin{aligned} \delta \int \kappa ds &= - \int \tau^2 \Omega_2 ds, \\ \delta \int \kappa \tau ds &= \int \left[\tau_{ss} + 2 \left(\frac{\kappa_s}{\kappa} \right)_s \tau + \frac{\kappa_s \tau_s}{\kappa} + \tau(2\kappa^2 - \tau^2) \right] \Omega_2 ds, \\ \delta \int \kappa^2 ds &= \int (2\kappa_{ss} + \kappa^3 - 2\kappa\tau^2) \Omega_2 ds \\ \text{and} \quad \delta \int \tau^2 ds &= \int \left[4 \left(\frac{\tau_s}{\kappa} \right)_s \tau + \frac{2\tau_s^2}{\kappa} + 3\kappa\tau^2 \right] \Omega_2 ds, \end{aligned} \right\} \quad (3.20)$$

with

$$\kappa_s = \frac{d\kappa}{ds}, \quad \tau_s = \frac{d\tau}{ds}, \quad \kappa_{ss} = \frac{d^2\kappa}{ds^2} \quad \text{and} \quad \tau_{ss} = \frac{d^2\tau}{ds^2}.$$

Substituting equations (3.13) and (3.20) into equation (3.16) leads to

$$\begin{aligned} \delta\Pi &= \frac{1}{2} \int \left\{ Q_0\kappa - Q_1\tau^2 + Q_2\kappa^3 + 2Q_3\kappa^2\tau + (3Q_4 - 2Q_2)\kappa\tau^2 - Q_3\tau^3 \right. \\ &\quad - Q_3\tau^3 + 2Q_2\kappa_{ss} + Q_3 \left[\tau_{ss} + 2 \left(\frac{\kappa_s}{\kappa} \right)_s \tau + \frac{\kappa_s \tau_s}{\kappa} \right] \\ &\quad \left. + Q_4 \left[4 \left(\frac{\tau_s}{\kappa} \right)_s \tau + \frac{2\tau_s^2}{\kappa} \right] \right\} \Omega_2 ds. \end{aligned} \quad (3.21)$$

Using $\delta \mathbf{r} = \Omega_3 \mathbf{e}_3$ in conjunction with the following relations (Tu *et al.* 2006)

$$\left. \begin{aligned} \delta ds &= \Omega_3 w_{31} = 0, & \Omega_{23} ds &= \frac{1}{\kappa} [2d(\tau\Omega_2) - \Omega_2 d\tau], \\ \delta \kappa ds &= d\Omega_{12} + (\kappa^2 - \tau^2)\Omega_2 ds & \text{and} & \delta \tau ds = d\Omega_{23} + 2\kappa\tau d\Omega_2, \end{aligned} \right\} \quad (3.22)$$

one obtains

$$\left. \begin{aligned} \delta \int \kappa ds &= \int \tau_s \Omega_3 ds, & \delta \int \tau ds &= - \int \kappa_s \Omega_3 ds, \\ \delta \int \kappa \tau ds &= \int \left[3\tau\tau_s - 2\kappa\kappa_s + \frac{\kappa_s}{\kappa} \tau^2 - \left(\frac{\kappa_s}{\kappa} \right)_{ss} \right] \Omega_3 ds, \\ \delta \int \kappa^2 ds &= \int (3\kappa_s \tau + \kappa \tau_s) \Omega_3 ds \\ \text{and} & & \delta \int \tau^2 ds &= \int 2 \left[\frac{\tau_s}{\kappa} \tau^2 - (\tau\kappa)_s - \left(\frac{\tau_s}{\kappa} \right)_{ss} \right] \Omega_3 ds. \end{aligned} \right\} \quad (3.23)$$

From equation (3.9), one has

$$\begin{aligned} \delta \Pi &= \frac{1}{2} \int \left\{ Q_1 \tau_s + (3Q_2 - 2Q_4) \kappa_s \tau + (Q_2 - 2Q_4) \kappa \tau_s \right. \\ &\quad \left. + Q_3 \left[3\tau_s \tau - 2\kappa_s \kappa - \left(\frac{\kappa_s}{\kappa} \right)_{ss} + \frac{\kappa_s}{\kappa} \tau^2 \right] + 2Q_4 \left[\frac{\tau_s}{\kappa} \tau^2 - \left(\frac{\tau_s}{\kappa} \right)_{ss} \right] \right\} \Omega_3 ds. \end{aligned} \quad (3.24)$$

Because Ω_2 and Ω_3 are arbitrary functions, the general equations governing the shape of quasi-one-dimensional nanomaterials at equilibrium are derived from equations (3.21) and (3.24) as

$$\begin{aligned} Q_0 \kappa - Q_1 \tau^2 + Q_2 \kappa^3 + 2Q_3 \kappa^2 \tau + (3Q_4 - 2Q_2) \kappa \tau^2 - Q_3 \tau^3 \\ + 2Q_2 \kappa_{ss} + Q_3 \left[\tau_{ss} + 2 \left(\frac{\kappa_s}{\kappa} \right)_s \tau + \frac{\kappa_s \tau_s}{\kappa} \right] + Q_4 \left[4 \left(\frac{\tau_s}{\kappa} \right)_s \tau + \frac{2\tau_s^2}{\kappa} \right] = 0, \end{aligned} \quad (3.25)$$

$$\begin{aligned} Q_1 \tau_s + (3Q_2 - 2Q_4) \kappa_s \tau + (Q_2 - 2Q_4) \kappa \tau_s \\ + Q_3 \left[3\tau_s \tau - 2\kappa_s \kappa - \left(\frac{\kappa_s}{\kappa} \right)_{ss} + \frac{\kappa_s}{\kappa} \tau^2 \right] + 2Q_4 \left[\frac{\tau_s}{\kappa} \tau^2 - \left(\frac{\tau_s}{\kappa} \right)_{ss} \right] = 0. \end{aligned} \quad (3.26)$$

For a binormal nanohelix, both the curvature and the twist are constant and can be expressed in terms of the shape parameters, i.e. the helical radius R and the helical angle φ . That is,

$$\kappa = \cos^2 \frac{\varphi}{R}, \quad \tau = \sin \varphi \cos \frac{\varphi}{R}. \quad (3.27)$$

Submitting equation (3.27) into (3.25) leads to the following shape equation for a binormal nanohelix:

$$\begin{aligned} Q_0 R^2 - Q_1 R \sin^2 \varphi + Q_2 \cos^4 \varphi + Q_3 \sin \varphi \cos \varphi (1 + \cos^2 \varphi) \\ + (3Q_4 - 2Q_2) \sin^2 \varphi \cos^2 \varphi = 0. \end{aligned} \quad (3.28)$$

In this case, equation (3.26) is automatically satisfied.

The centreline of a nanohelix can also be described by

$$\mathbf{r}(s) = R \cos(\lambda s) \mathbf{e}_1 + R \sin(\lambda s) \mathbf{e}_2 + h_0 \lambda s \mathbf{e}_3, \quad (3.29)$$

where $\lambda = 1/\sqrt{\kappa^2 + \tau^2}$ and $P = 2\pi h_0$. Here, one has

$$\kappa = \frac{R}{R^2 + h_0^2} \quad \text{and} \quad \tau = \frac{h_0}{R^2 + h_0^2}. \quad (3.30)$$

Then, the shape equation (3.28) is recast as

$$\begin{aligned} Q_0 R^5 + (2Q_0 h_0^2 + Q_2) R^3 - (Q_1 h_0 - 2Q_3) h_0 R^2 - (Q_1 h_0 + Q_3) h_0^3 \\ + (Q_0 h_0^2 - 2Q_2 + 3Q_4) h_0^2 R = 0. \end{aligned} \quad (3.31)$$

From equations (3.13) and (3.27), the potential energy of a binormal nanohelix is obtained as

$$\begin{aligned} \Pi = \frac{L}{2R^2} (-Q_0 R^2 + Q_1 R \cos^2 \varphi + Q_2 \cos^4 \varphi + Q_3 \sin \varphi \cos^3 \varphi \\ + Q_4 \sin^2 \varphi \cos^2 \varphi). \end{aligned} \quad (3.32)$$

The stable condition of a binormal nanohelix reads

$$\delta^2 \Pi = \int_0^L \left(\sum_{i,j=1,2} \frac{\partial^2 H_0}{\partial \eta_i \partial \eta_j} \delta \eta_i \delta \eta_j \right) ds > 0, \quad (3.33)$$

where $\eta_1 = R$ and $\eta_2 = \varphi$. Equation (3.33) needs the positive determinant of the Hessian matrix $S = \det |\partial^2 H_0 / \partial \eta_i \partial \eta_j|$ (Zhou *et al.* 2005; Tu *et al.* 2006). For a binormal nanohelix, S is a constant and can be obtained easily.

For a nanowire with isotropic surfaces, the potential energy function takes the following form:

$$\Pi = \frac{1}{2} \int [B_0^* \kappa^2(s) + C_0^* \tau^2(s) - E b h \varepsilon_0^2] ds + \int m_0 ds, \quad (3.34)$$

where m_0 denotes an anisotropic or non-symmetrical external stimulus associated with growth or constraints. m_0 can be induced by, for instance, the anisotropic contact between the nanowire and the catalyst (Fonseca *et al.* 2007). The coefficients B_0^* and C_0^* are expressed as

$$B_0^* = B_1 + \frac{1}{2} E^s b h^2 \quad \text{and} \quad C_0^* = C_1 + \frac{1}{2} G^s b h^2, \quad (3.35)$$

where E^s and G^s are the surface elastic modulus and surface shear modulus, respectively. In general, both the effective bending rigidity B_0^* and torsional rigidity C_0^* are positive.

Analogous to the derivation of equations (3.25) and (3.26), the governing equations for the equilibrium shape of a nanowire with isotropic surfaces are obtained as

$$2B_0^* \kappa_{ss} + B_0^* \kappa^3 + (3C_0^* - 2B_0^*) \kappa \tau^2 + 4C_0^* \left(\frac{\tau_s}{\kappa} \right) \tau + 2C_0^* \frac{\tau_s^2}{\kappa} - E b h \varepsilon_0^2 - 2m_0 = 0 \quad (3.36)$$

and $(2B_0^* - C_0^*) \kappa_s \tau + (B_0^* - C_0^*) \kappa \tau_s + C_0^* \left[\frac{\tau_s}{\kappa} \tau^2 - \left(\frac{\tau_s}{\kappa} \right)_{ss} \right] = 0. \quad (3.37)$

From equation (3.36), the corresponding shape equation for a nanohelix is obtained as

$$B_0^* R^2 + (3C_0^* - 2B_0^*) h_0^2 - E b h \varepsilon_0^2 (R^2 + h_0^2)^2 - 2m_0 (R^2 + h_0^2)^2 = 0. \quad (3.38)$$

Generally, equation (3.38) can have non-trivial solutions, meaning that a nanowire with isotropic surface property can also admit a helical shape as a result of external stimuli, e.g. forces, temperature, growth or shrinkage, which may present during fabrication. However, in the case of the isotropic surfaces with $m_0 = 0$, the nanowires will not bend and twist to form the nanohelices after the release of the axial residual strain. In other words, the mere uniform release of axial residual strain or stress cannot lead to the formation of a helical shape of nanowires with isotropic surface properties. In this circumstance, the formation of a helical morphology requires the presence of anisotropic external stimuli, e.g. non-symmetrical forces and anisotropic contact between the catalyst and the nanowire during the growth or fabrication process. On the other hand, the above theoretical analysis shows that, for nanowires with anisotropic surface properties, the axial deformation, twisting and bending are usually coupled, rendering the appearance of helical or more complex shapes. Therefore, the presence of unbalanced residual surface stresses plays an important role in the formation of such asymmetric shapes.

4. Discussion

(a) Comparison with relevant experiments

In §3, we have proposed an anisotropic surface stress mechanism for the formation of chiral morphologies, and the corresponding shape equations have been derived as equations (3.4) and (3.28). This physical mechanism can explain why many nanowires in practical fabrication often assume complicated morphologies with chirality, e.g. twisting and bending morphologies and their assemblies. Here, we use our recent experiments of polymer lamellae (Ye *et al.* 2010) to validate these kinds of surface effects. Their chiral morphologies are successfully controlled and tuned by varying the anisotropic surface stresses with a chemical method (Ye *et al.* 2010).

Microscopic observations have revealed that polymer spherulites are composed of stacks or aggregations of nanosized twisted lamellae (Xu *et al.* 2004; Lotz & Cheng 2005; Ye *et al.* 2010). These lamellae grow radially from the centre of the spherulite and usually twist with a definite pitch, as shown in figure 4a (Ye *et al.* 2010). As we have pointed out already, the surface stresses play a

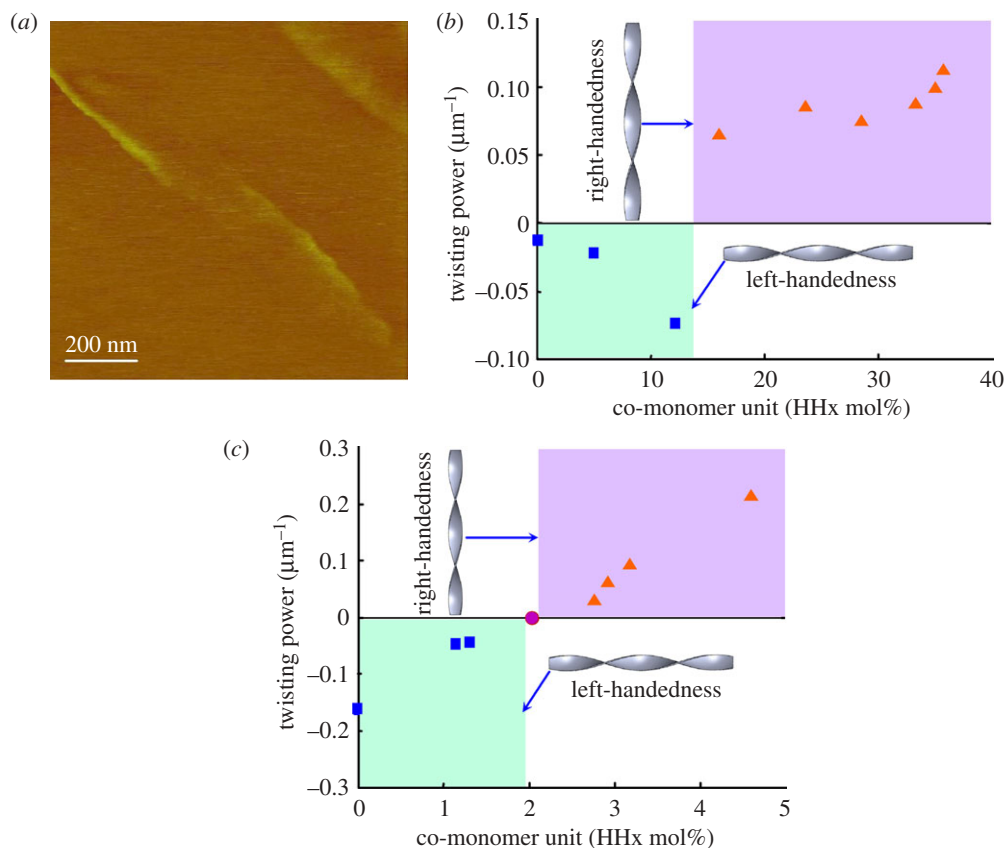


Figure 4. Experimental results on the tuning of the twisting handedness of polymer lamellae. (a) An individual twisting lamellar crystal in PHBHHx-17 thin film, crystallized at 85°C . Yellow represents the twisting polymer lamellar crystal, and dark red represents the substrate film in which the polymer lamellae crystallized. (b) PHBV random copolymers. (c) Blends of PHB with PHBHHx-4.6. The co-monomer content is adjusted by changing the blend ratio of the two components, which are miscible in the melt and will not phase-separate during crystallization. The twisting power is the reciprocal of the twisting pitch. Right-handed twisting (squares) is defined to be positive and left-handed twisting (triangles) is negative (Ye *et al.* 2010).

crucial role in the formation of chiral morphologies of nanomaterials, especially for such soft materials as polymer lamellae. The twisting growth of polymer lamellae can be attributed to the surface stresses induced by oriented chain folding. We took chiral microbial poly(*R*-3-hydroxybutyrate) (PHB) copolymer as an example. Surface treatments to the polymer lamellae are performed by copolymerization or bending, as described in our previous work (Ye *et al.* 2010). Wide angle X-ray diffraction results demonstrate that the technique of copolymerization or bending does not change the composition and structure of the crystalline core, but changes only the surface layer microstructure and the corresponding anisotropic surface stresses (Ye *et al.* 2010). By this method, we successfully tuned the twisting pitch length and the lamellar twisting chirality of the microbial PHB copolymer lamellae from the left-handed chirality to the right-handed chirality, as shown in figure 4*b,c*. The principal directions and

magnitudes of the surface stresses in the nanosized lamellae depend mainly on the oriented chain folding and the added co-monomer, and they vary with the addition of co-monomer. The lamellar core has the same crystalline structure before and after the surface treatment. Therefore, the variation and inversion of twisting chirality shown in figure 4 are clearly attributed to the changes in anisotropic surface stresses. As can be seen from figure 4*b,c*, both the twisting chirality and the twisting pitch length show remarkable changes as the content of the co-monomer increases. For poly(*R*-3-hydroxybutyrate-co-*R*-3-hydroxyvalerate) (PHBV) random copolymer crystals, the twisting pitch length first increases and then decreases after the twisting chirality has been inverted from left-handedness to right-handedness. While for the blended crystal of PHB with poly(*R*-3-hydroxybutyrate-co-*R*-3-hydroxyhexanoate) random copolymer (PHBHHx) with 4.6 mol% 3-hydroxyhexanoate (HHx) content (PHBHHX-4.6), the twisting pitch length increases to infinite and there is no twisting deformation with increasing co-monomer content. With the inversion of the twisting chirality from left- to right-handedness, the twisting pitch length is also changed. Figure 4*b,c* verifies that the anisotropic surface stresses tuned by the surface treatment can change not only the twisting chirality of the polymer lamellae but also their pitch length, as has been predicted by our theory in §3 (Wang *et al.* 2008). In addition, our experiments showed that, for the twisting lamellar crystal of poly(*R*-3-hydroxyvalerate), the twisting along different radial directions can also lead to opposite twisting handedness (Ye *et al.* 2009). These experiments demonstrate the significant role of the anisotropic feature of surface stresses in the formation of chiral morphologies of quasi-one-dimensional nanomaterials.

(b) Analysis of twisting nanowires

In this subsection, we numerically illustrate the effect of anisotropic surface properties on the formation of twisting nanowires and the associated size effect. We consider a thin nanowire (or nanoribbon) of thickness h and width b . Assume that its front and back surfaces have different orthotropic elastic properties, which are characterized in terms of the orientation angles θ^\pm of the principal axes, the anisotropy degrees A_0^\pm and the constants a^\pm (Wang *et al.* 2008). The anisotropic surface stresses induced by the differences in θ^\pm , A_0^\pm and a^\pm can bend and twist the nanowire into a helical shape. The orthotropic elastic constitutive relations of the surfaces are written as (Quang & He 2007; Wang *et al.* 2008)

$$\left. \begin{aligned} c_{1111}^{s\pm} &= c_{2222}^{s\pm} = \lambda_s + a^\pm \mu_s, \\ c_{1122}^{s\pm} &= c_{2211}^{s\pm} = \lambda_s - a^\pm \mu_s \\ \text{and} \quad c_{1212}^{s\pm} &= c_{1221}^{s\pm} = \frac{1}{2} A_0^\pm (c_{1111}^{s\pm} - c_{1122}^{s\pm}), \end{aligned} \right\} \quad (4.1)$$

where λ_s and μ_s designate the surface elastic moduli, and a_1^\pm are dimensionless constants. The parameters A_0^+ and A_0^- stand for the degree of anisotropy of surface elasticity in the front and back surfaces, respectively.

In the example, we take the following representative values of material parameters for the bulk and surface properties of the polymer lamella (Ye *et al.* 2010): $E = 6.1$ GPa (Owen 1997), $\nu = 0.4$, $A_0^+ = A_0^- = 0.1$ and $a^+ = a^- = 1.0$. The surface parameters obtained from equations (2.5) and (4.1) are assumed

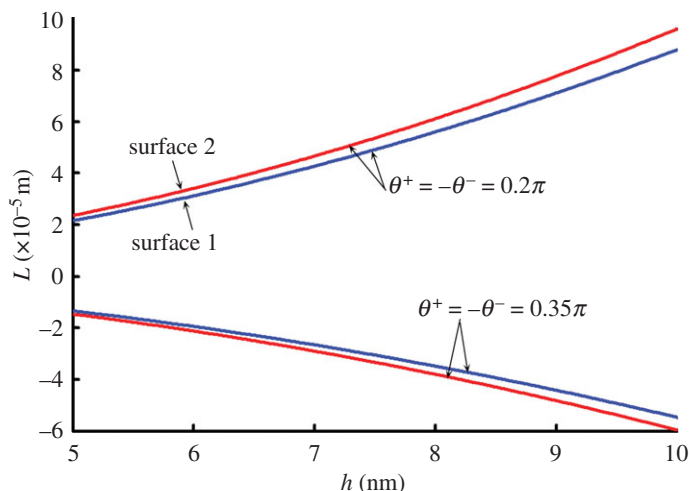


Figure 5. Variation of the half-twisting period length of a polymer lamella with respect to its thickness. (Online version in colour.)

to be mainly attributed to the variation of θ^\pm , which can be approximately determined based on the chain-folding structures on the front and back surfaces of the polymer lamellae. Based on the twisting and bending deformations of the full polymer lamellae and the half polymer lamellae, surface elastic moduli are taken as surface 1: $\lambda_s = -2.7285 \text{ N m}^{-1}$ and $\mu_s = -6.2178 \text{ N m}^{-1}$; and surface 2: $\lambda_s = 3.49387$ and $\mu_s = -5.70915 \text{ N m}^{-1}$ (Ye *et al.* 2010). For the polymer lamellae, the twisting pitch length may vary from several hundred nanometres to several hundred microns, depending on such factors as synthesis conditions. For example, our experiments showed that the thickness and pitch length of the twisting PHBV random copolymer lamellae mainly vary in the range of 6–8 nm and 6–82 μm , respectively.

The theoretical predication for the twisting pitch length of the polymer lamellae is plotted in figure 5, which has a good agreement with relevant experimental results. It is reasonable to find that the half-twisting pitch lengths vary with the lamellar thickness h . In addition, the twisting shape of the lamellae can be changed from the right-handedness for the case of $\theta^+ = -\theta^- = 0.2\pi$ to the left-handedness for the case of $\theta^+ = -\theta^- = 0.35\pi$. Therefore, the theoretical results of the twisting pitch length and the twisting sense inversion agree well with our experimental results, demonstrating the significant effects of anisotropic surface stresses on the formation of twisting morphologies. It should be mentioned that the residual surface stresses may be anisotropic and different in the front and back surfaces while the elastic modulus of the two surfaces can remain isotropic. In this case, the nanowires can also be twisted, and can be similarly analysed.

Furthermore, it can be seen that the twisting pitch length and the twisting sense of a nanobelt depend on its surface properties and cross-sectional size. In other words, the chiral morphology induced by surface effects exhibits distinct size dependence, and the effects of surface stresses and surface elasticity on the morphology of materials will become insignificant at macro-scale. It is worth noting that, besides the straight twisting nanobelts, anisotropic surface effects can

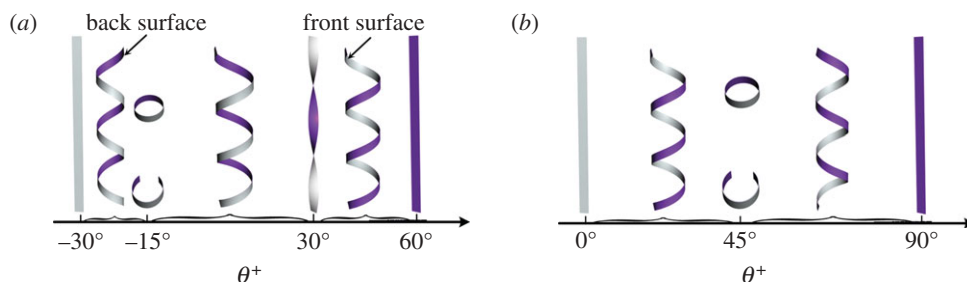


Figure 6. Variation of the chiral morphologies of nanowires with respect to the orientation angle θ^+ of the anisotropic constitutive relation of the surface layer: (a) $\theta^- = 30^\circ$ and (b) $\theta^- = 0^\circ$. (Online version in colour.)

also induce the bent twisting nanobelts such as half polymer lamellae, rendering much more complicated morphologies of quasi-one-dimensional nanomaterials, as observed in our experiments (Ye *et al.* 2010).

(c) Analysis of nanohelices

For a nanohelix with anisotropic surface stresses, the equilibrium shape equation in equation (3.28) or (3.31) provides the dependence relationship of its helical angle and radius on the elastic properties of the surface and bulk materials and the cross-sectional geometric parameters. An equilibrium shape should be stable and energetically favourable; in other words, equation (3.15) should be satisfied.

Under given anisotropic surface properties, the handedness of a chiral nanohelix or twisting nanobelt can be easily determined according to the above theory. For the sake of simplicity, we assume in the following example that the two main surfaces of a nanoribbon have the same orthotropic elastic properties but different orientation angles. A schematic phase diagram is given in figure 6a to show the dependence of the chiral shape on the orientation angle, where we vary only the value of θ^+ but fix the other surface parameters as $\theta^- = -30^\circ$, $A_0^\pm = 0.2$ and $a^\pm = 1.0$, $\lambda_s = -2.7285$ and $\mu_s = -6.2178 \text{ N m}^{-1}$ (Shenoy 2002). When $\theta^+ = \theta^-$, the nanowire is straight because the surface stresses in the front and back surfaces are identical and balanced. When $\theta^+ = -15^\circ$, we have $c_{32}^+ = c_{32}^-$, $c_{22}^+ \neq c_{22}^-$, and the nanowires will only have bending deformation, as shown in figure 6a. When $\theta^+ = -\theta^- = 30^\circ$, we have $c_{32}^+ = -c_{32}^-$ and $c_{22}^+ = c_{22}^-$. In this case, the material will not bend but twist, rendering the formation of twisting nanobelts. For other values of θ^+ , one has $|c_{32}^+| \neq |c_{32}^-|$ and $c_{22}^+ \neq c_{22}^-$. Thus, the surface stresses will simultaneously bend and twist the nanowire into a nanohelix of left- or right-handedness. The bending direction of the nanowires when $-30^\circ < \theta^+ < 30^\circ$ is contrary to that when $30^\circ < \theta^+ < 60^\circ$ owing to the different values of c_{22}^+ and c_{22}^- . In addition, the chiral morphology of nanowires exhibits a periodic dependence on the increasing value of θ^+ . Figure 6b schematically shows the phase diagram of nanowires with $\theta^- = 0^\circ$. It is interesting to note that, when $\theta^- = 0^\circ$, no twisting nanobelt can be formed.

Under other combinations of θ^+ and θ^- , the morphology of a nanowire can also be determined, but this is omitted in figure 6. It may have a right- or left-handed chirality, depending on whether $c_{32}^+ - c_{32}^- > 0$ or $c_{32}^+ - c_{32}^- < 0$. Furthermore, some

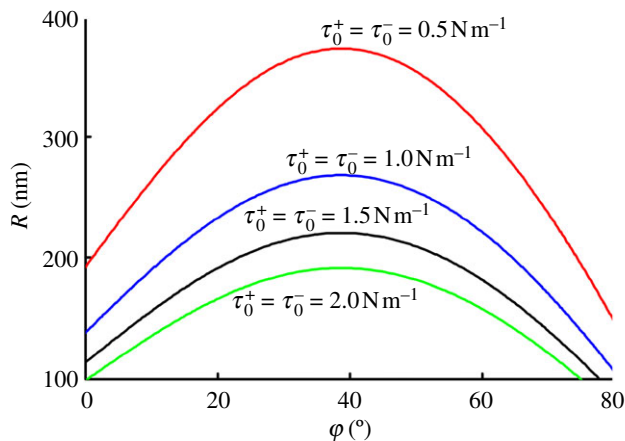


Figure 7. Effect of the residual surface stresses on the R - φ relation of the helical nanowire. (Online version in colour.)

Table 1. Elastic properties of the surface and bulk and the geometric size of a nanowire.

parameter	E (GPa)	ν	λ_s (N m^{-1})	μ_s (N m^{-1})	θ^+ ($^\circ$)	θ^- ($^\circ$)	A_0^\pm	a_0^\pm	h (nm)	b (nm)
value	6.1	0.4	-2.7285	-6.2178	30	0	-0.3	1.0	10	50

other chiral morphologies (e.g. coils and helical tubes) can also be formed for nanowires with different surface properties, which can be readily analysed by the present model but are omitted here for conciseness.

Besides the handedness, the chiral shapes of nanowires caused by residual surface stresses or surface eigenstresses are also investigated. From equation (3.28), the variation of the helical radius R with the helical angle φ is plotted in figure 7 under four different values of τ_0^\pm . In the figure, we take $\varepsilon_0 = 0.009$, and the other parameters are listed in table 1. For simplicity, it is assumed that $\tau_0^+ = \tau_0^-$. A positive value of the helical angle φ ($0^\circ < \varphi < 90^\circ$) represents the right-handed chirality of the nanohelix, while a negative value of φ ($-90^\circ < \varphi < 0^\circ$) represents the left-handedness. It is seen that, when the residual surface stresses or surface eigenstresses have larger positive values, the nanowire will have larger bending and twisting deformation, leading to the formation of a nanohelix with smaller helical radius.

The relation between the helical radius R and the helical angle φ is shown in figure 8, where we use $\theta^+ = 10^\circ, 20^\circ, 30^\circ, 40^\circ$, and the other material parameters are listed in table 1. Under the specified material parameters, the helical radius R decreases with increasing φ in the range of $40^\circ < \varphi < 80^\circ$, whereas, for coiled nanohelices in the range of $0^\circ < \varphi < 10^\circ$, a larger value of θ^+ will induce a larger helical radius. For other combinations of material and geometric parameters, the chiral morphologies can also be easily predicted by the present theory.

In figure 9, we examine the effect of the anisotropy degree of the surface layers on the R - φ relation, where the parameters in table 1 have been used. A stronger anisotropy degree of surface elasticity often induces a larger helical

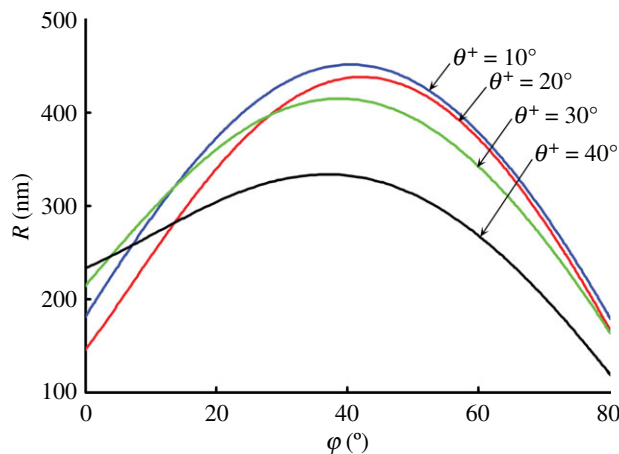


Figure 8. The relation between the helical radius R and the helical angle φ of a nanoribbon under different values of the orientation angle θ^+ . (Online version in colour.)

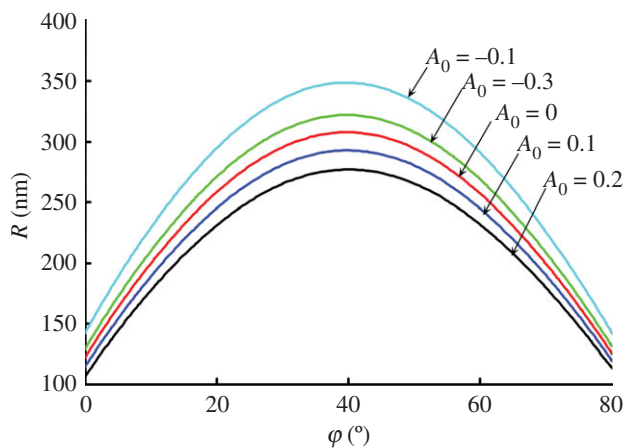


Figure 9. The relation between the helical radius R and the helical angle φ of a nanoribbon under different surface elastic constants. (Online version in colour.)

radius under a given helical angle. The helical radius first increases and then decreases with the increase in φ . Besides the surface parameters, the elastic properties of the bulk material also have a significant influence on the equilibrium shapes of the nanomaterials. For example, figure 10 shows the influence of Young's modulus E on the morphology of nanohelices under the surface elastic properties and geometric sizes listed in table 1. For a coiled nanohelix, a larger Young's modulus usually leads to a larger helical radius owing to the stiffening effect of the core. When $\varphi > 15^\circ$, the helical radius will be decreased with increasing Young's modulus.

Finally, we examine the dependence of the chiral morphology of a nanowire on its cross-sectional sizes. Under several representative thicknesses of the nanowire, the R - φ curves are given in figure 11, where we set $A_0^\pm = -0.1$ and the other elastic

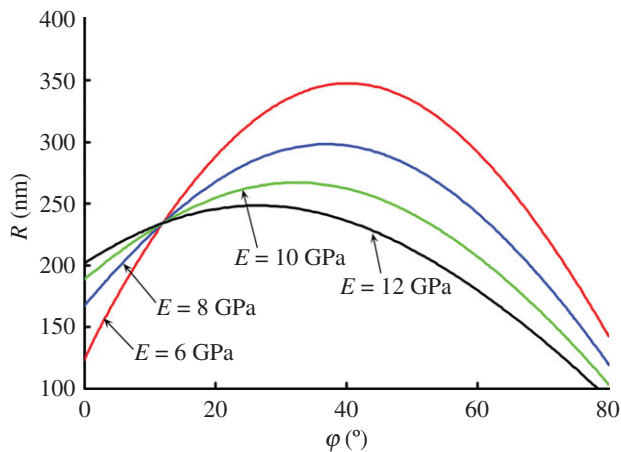


Figure 10. Effect of Young's modulus of the bulk material on the R - ϕ relation of the helical nanowire. (Online version in colour.)

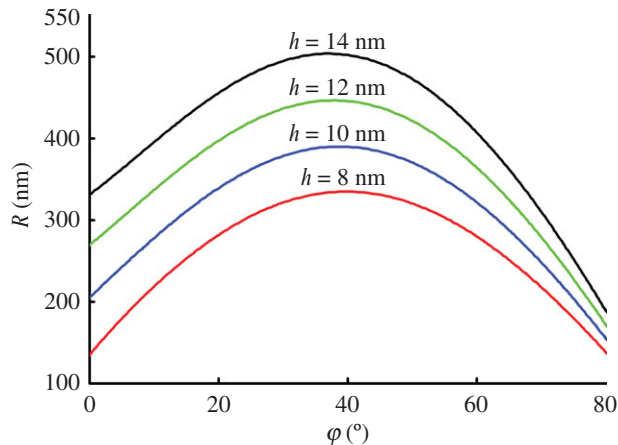


Figure 11. Effect of the thickness on the R - ϕ relation of the helical nanowire. (Online version in colour.)

properties of the surfaces and the bulk are as shown in [table 1](#). It is found that, for nanohelices with a smaller helical angle $\phi < 40^\circ$, the helical radius R increases with increasing ϕ . While for nanohelices with a large helical angle $\phi > 40^\circ$, the helical radius decreases with ϕ . Furthermore, a thinner nanowire normally assumes a smaller helical radius. Therefore, the chiral morphology of a nanowire exhibits distinct dependence on its cross-sectional size.

5. Conclusions

In this study, we have developed a refined Kirchhoff rod model for studying nanowires with anisotropic surface effects. It is used to investigate the formation of chiral morphologies of quasi-one-dimensional nanomaterials. Our analysis

demonstrates that anisotropic surface stresses can engender the formation of various complicated morphologies of nanomaterials, e.g. twisting and bending nanobelts and nanohelices. Using the variational method of energy, the general equations controlling the equilibrium shape of nanowires are derived. Our analysis shows that such geometric parameters as the helical angle, helical radius and pitch length of chiral morphologies induced by anisotropic stresses depend on the elastic properties of surface and bulk materials as well as the cross-sectional sizes of the nanowire. Anisotropic surface stresses can induce the formation of binormal helical shapes, but not normal helical shapes. These results suggest that nanobelts or nanoribbons of various spatial shapes can be fabricated and even modulated by tailoring or functionalizing their surfaces. In addition, this model can also be applied to analyse the presence of self-assembled helical ribbons and biological systems such as the spiral flagella of bacteria and the helical virus. The application of this method in the biological field is underway. Finally, it is emphasized that there exist some other factors (e.g. dislocations and asymmetric growth and chirality transfer; Wang *et al.* 2011) that affect the morphologies of nanomaterials, and the coupling analysis of surface effects and these mechanisms will be of great interest.

Support from the National Natural Science Foundation of China (grant nos. 10732050, 10572076, 10802041 and 20974060), 973 Programme (2010CB631005 and 2012CB934101), the China Postdoctoral Science Foundation and the Innovation Foundation of Tianjin University is acknowledged. The authors thank Professors Zongxi Cai and Ganyun Huang for their helpful discussions and the anonymous reviewers for their helpful comments and suggestions.

References

- Amelinckx, S., Zhang, X. B., Bernaerts, D., Zhang, X. F., Ivanov, V. & Nagy, J. B. 1994 A formation mechanism for catalytically grown helix-shaped graphite nanotubes. *Science* **265**, 635–639. (doi:10.1126/science.265.5172.635)
- Bandaru, P. R., Daraio, C., Yang, K. & Rao, A. M. 2007 A plausible mechanism for the evolution of helical forms in nanostructure growth. *J. Appl. Phys.* **101**, 094307. (doi:10.1063/1.2723189)
- Cahill, K. 2005 Helices in biomolecules. *Phys. Rev. E* **72**, 062901. (doi:10.1103/PhysRevE.72.062901)
- Chen, X. Q., Yang, S. M. & Motojima, S. 2005 Morphology and microstructure of twisting nanoribbons prepared using sputter-coated Fe-base alloy catalysts on glass substrates. *Mater. Lett.* **59**, 854–858. (doi:10.1016/j.matlet.2004.10.065)
- Dingreville, R., Qu, J. M. & Cherkaoui, M. 2005 Surface free energy and its effect on the elastic behavior of nano-sized particles, wires and films. *J. Mech. Phys. Solids* **53**, 1827–1854. (doi:10.1016/j.jmps.2005.02.012)
- Duan, H. L., Wang, J., Huang, Z. P. & Karimhaloo, B. L. 2005 Eshelby formalism for nano-inhomogeneities. *Proc. R. Soc. A* **461**, 3335–3353. (doi:10.1098/rspa.2005.1520)
- Fonseca, A. F. D. & Galvão, D. S. 2004 Mechanical properties of nanosprings. *Phys. Rev. Lett.* **92**, 1755021. (doi:10.1103/PhysRevLett.92.175502)
- Fonseca, A. F. D., Malta, C. P. & Galvão, D. S. 2007 Is it possible to grow amorphous normal nanosprings? *Nanotechnology* **18**, 435606. (doi:10.1088/0957-4484/18/43/435606)
- Gao, X. P., Ding, Y., Mai, W. J., Hughes, W. L., Lao, C. S. & Wang, Z. L. 2005 Conversion of zinc oxide nanobelts into superlattice-structured nanohelices. *Science* **309**, 1700–1704. (doi:10.1126/science.1116495)
- Gao, L. T., Feng, X. Q., Yin, Y. J. & Gao, H. J. 2008 An electromechanical liquid crystal model of vesicles. *J. Mech. Phys. Solids* **59**, 2844–2862. (doi:10.106/j.jmps.2008.04.006)

- Gibbs, J. W. 1928 *The collected works of J. Willard Gibbs*. New York, NY: Longmans.
- Goriely, A. & Neukirch, S. 2006 Mechanics of climbing and attachment in twining plants. *Phys. Rev. Lett.* **97**, 184302. (doi:10.1103/PhysRevLett.97.184302)
- Gurtin, M. E. & Murdoch, A. I. 1975 A continuum theory of elastic material surfaces. *Arch. Ration. Mech. Anal.* **57**, 291–323.
- Gurtin, M. E., Weissmüller, J. & Larché, F. 1995 A general theory of curved deformable interface in solids at equilibrium. *Phil. Mag. A* **78**, 1093–1109. (doi:10.1080/01418619808239977)
- He, L. H., Lim, C. W. & Wu, B. S. 2004 A continuum model for size-dependent deformation of elastic films of nano-scale thickness. *Int. J. Solids Struct.* **41**, 847–857. (doi:10.1016/j.ijsolstr.2003.10.001)
- Huang, G. Y. & Kang, Y. L. 2011 Acoustic vibrations of a circular nanowire by considering the effect of surface. *J. Appl. Phys.* **110**, 023526. (doi:10/1063/1.3610498)
- Hütter, M., Veld, P. J. I. & Rutledge, G. C. 2006 Polyethylene {201} crystal surface: interface stresses and thermodynamics. *Polymer* **47**, 5494–5504. (doi:10.1016/j.polymer.2005.05.160)
- Khaykovich, B., Hossain, C., McManus, J. J., Lomakin, A., Moncton, D. E. & Benedek, G. B. 2007 Structure of cholesterol helical ribbons and self-assembling biological springs. *Proc. Natl Acad. Sci. USA* **104**, 9656–9660. (doi:10/1073/pans.00702967 104)
- Kim, M. J. & Powers, T. R. 2005 Deformation of a helical filament by flow and electric or magnetic fields. *Phys. Rev. E* **71**, 021914. (doi:10.1103/PhysRevE.71.021914)
- Kim, H. W. & Shim, S. H. 2007 Helical nanostructures of SiO_x synthesized through the heating of co-coated substrates. *Appl. Surf. Sci.* **253**, 3664–3668. (doi:10.1016/j.apsusc.2006.07.083)
- Kong, X. Y. & Wang, Z. L. 2003 Spontaneous polarization-induced nanohelices, nanosprings, and nanorings of piezoelectric nanobelts. *Nano Lett.* **3**, 1625–1631. (doi:10.1021/nl034463p)
- Korgel, B. A. 2005 Nanosprings take shape. *Science* **309**, 1683–1684. (doi:10.1126/science.1118125)
- Liu, Y. Z. 2006 *Nonlinear mechanics of thin elastic rod: theoretical basics of mechanical model of DNA*. Beijing, China: Tsinghua University Press.
- Lotz, B. & Cheng, S. Z. D. 2005 A critical assessment of unbalanced surface stresses as the mechanical origin of twisting and scrolling of polymer crystals. *Polymer* **46**, 577–610. (doi:10.1016/j.polymer.2004.07.042)
- Lu, W. & Suo, Z. 2002 Symmetry breaking in self-assembled monolayers on solid surfaces: anisotropic surface stress. *Phys. Rev. B* **65**, 085401. (doi:10.1103/PhysRevB.65.085401)
- Lu, P., He, L. H., Lee, H. P. & Lu, C. 2006 Thin plate theory including surface effects. *Int. J. Solids Struct.* **43**, 4631–4647. (doi:10.1016/j.ijsolstr.2005.07.036)
- McIlroy, D. N., Zhang, D. & Kranov, Y. 2001 Nanosprings. *Appl. Phys. Lett.* **79**, 1540–1542. (doi:10.1063/1.1400079)
- Middel, M. T., Zandvliet, H. J. W. & Poelsema, B. 2002 Surface stress anisotropy of Ge(001). *Phys. Rev. Lett.* **88**, 196105. (doi:10.1103/PhysRevLett.88.196105)
- Miller, R. E. & Shenoy, V. B. 2000 Size-dependent elastic properties of nanosized structural elements. *Nanotechnology* **11**, 139–147. (doi:10.1088/0957-4484/11/3/301)
- Ou-Yang, Z. C. & Su, Z. B. 1997 Coil formation in multishell carbon nanotubes: competition between curvature elasticity and interlayer adhesion. *Phys. Rev. Lett.* **78**, 4055–4058. (doi:10.1103/PhysRevLett.78.4055)
- Owen, J. A. 1997 A note on twist-banding in spherulites of poly(3-hydroxybutyrate). *Polymer* **38**, 3705–3708. (doi:10.1016/S0032-3861(97)00037-2)
- Park, H. S. & Klein, P. A. 2008 Surface stress effects on the resonant properties of metal nanowires: the importance of finite deformation kinematics and the impact of the residual surface stress. *J. Mech. Phys. Solids* **56**, 3144–3166. (doi:10.1016/j.jmps.2008.08.003)
- Quang, H. L. & He, Q. C. 2007 Size-dependent effective thermoelastic properties of nanocomposites with spherically anisotropic phases. *J. Mech. Phys. Solids* **55**, 1889–1921. (doi:10.1016/j.jmps.2007.02.005)
- Ru, C. Q. 2010 Size effect of dissipative surface stress on quality factor of microbeams. *Appl. Phys. Lett.* **94**, 051905. (doi:10.1063/1.3078816)
- Sander, D., Enders, A. & Kirschner, J. 1999 Anisotropic surface stress on W(110). *Europhys. Lett.* **45**, 208–214. (doi:10.1209/epl/i1999-00148-y)

- Sharma, P., Ganti, S. & Bhate, N. 2003 Effect of surfaces on the size-dependent elastic state of nano-inhomogeneities. *Appl. Phys. Lett.* **82**, 535–537. (doi:10.1063/1.2234561)
- Shenoy, V. B. 2002 Size-dependent rigidities of nanosized torsional elements. *Int. J. Solids Struct.* **39**, 4039–4052. (doi:10.1016/S0020-7683(02)00261-5)
- Siegel, M., Miksis, M. J. & Voorhees, P. W. 2004 Evolution of material voids for highly anisotropic surface energy. *J. Mech. Phys. Solids* **52**, 1319–1353. (doi:10.1016/j.jmps.2003.11.003)
- Smith, B., Zastavker, Y. V. & Benedek, G. B. 2001 Tension-induced straightening transition of self-assembled helical ribbons. *Phys. Rev. Lett.* **87**, 278101. (doi:10.1103/PhysRevLett.87.278101)
- Snir, Y. & Kamien, R. D. 2005 Entropically driven helix formation. *Science* **307**, 1067. (doi:10.1126/science.1106243)
- Tian, L. & Rajapakse, R. K. N. D. 2007 Analytical solution for size-dependent elastic field of a nanoscale circular inhomogeneity. *Int. J. Solids Struct.* **44**, 7988. (doi:10.1115/1.2424242)
- Tu, Z. C., Li, Q. X. & Hu, X. 2006 Theoretical determination of the necessary conditions for the formation of ZnO nanorings and nanohelices. *Phys. Rev. B* **73**, 115402. (doi:10.1103/PhysRevB.73.115402)
- Wang, G. F., Feng, X. Q. & Yu, S. W. 2007 Surface buckling of a bending microbeam due to surface elasticity. *Europhys. Lett.* **77**, 44002. (doi:10.1209/0295-5075/77/44002)
- Wang, J. S., Feng, X. Q., Wang, G. F. & Yu, S. W. 2008 Twisting of nanowires induced by anisotropic surface stresses. *Appl. Phys. Lett.* **92**, 191901. (doi:10.1063/1.2928221)
- Wang, J. S., Cui, Y. H., Feng, X. Q., Wang, G. F. & Qin, Q. H. 2010 Surface effects on the elasticity of nanosprings. *Europhys. Lett.* **92**, 16002. (doi:10.1209/0295-5075/92/16002)
- Wang, J. S., Feng, X. Q., Xu, J., Qin, Q. H. & Yu, S. W. 2011 Chirality transfer from molecular to morphological scales in quasi-one-dimensional nanomaterials: a continuum model. *J. Comput. Theor. Nanosci.* **8**, 1278–1287. (doi:10.1166/jctn.2011.1811)
- Wang, Z. J., Liu, C., Li, Z. G. & Zhang, T. Y. 2010 Size-dependent elastic properties of Au nanowires under bending and tension: surface versus core nonlinearity. *J. Appl. Phys.* **108**, 083508. (doi:10.1063/1.3493264)
- Xia, R., Feng, X. Q. & Wang, G. F. 2011 Effective elastic properties of hierarchical nanoporous materials. *Acta Mater.* **59**, 6801–6808. (doi:10.1016/j.actamat.2011.07.039)
- Xu, J. *et al.* 2004 Direct AFM observation of crystal twisting and organization in banded spherulites of chiral poly(3-hydroxybutyrate-co-3-hydroxyhexanoate). *Macromolecules* **37**, 4118–4123. (doi:10.1021/ma0499122)
- Ye, H. M., Xu, J., Guo, B. H. & Iwata, T. 2009 Left- or right-handed lamellar twists in poly[(R)-3-hydroxyvalerate] banded spherulite: dependence on growth axis. *Macromolecules* **42**, 694–701. (doi:10.1021/ma801653p)
- Ye, H. M. *et al.* 2010 Surface stress effects on the bending direction and twisting chirality of lamellar crystals of chiral polymer. *Macromolecules* **43**, 5762–5770. (doi:10.1021/ma100920u)
- Zastavker, Y. V., Asherie, Z., Lomakin, A., Pande, J., Donovan, J. M., Schnur, J. M. & Benedek, G. B. 1999 Self-assembly of helical ribbons. *Proc. Natl Acad. Sci. USA* **96**, 7883–7887. (doi:10.1073/pnas.96.14.7883)
- Zhang, D. Q., Alkhateeb, A., Han, H. M., Mathmood, H. & McIlroy, D. N. 2003 Silicon carbide nanosprings. *Nano Lett.* **3**, 983–987. (doi:10.1021/nl034288c)
- Zhang, T. Y., Luo, M. & Chan, W. K. 2008 Size-dependent surface stress, surface stiffness, and Young's modulus of hexagonal prism [111] β -SiC nanowires. *J. Appl. Phys.* **103**, 104308. (doi:10.1063/1.2927453)
- Zhang, T. Y., Wang, Z. J. & Chan, W. K. 2010 Eigenstress model for surface stress of solids. *Phys. Rev. B* **81**, 195427. (doi:10.1103/PhysRevB.81.195427)
- Zhang, T. Y., Ren, H., Wang, Z. J. & Sun, S. 2011 Surface eigen-displacement and surface Poisson's ratios of solids. *Acta Mater.* **59**, 4437–4447. (doi:10.1016/j.actamat.2011.03.067)
- Zhao, S. M., Zhang, S. L., Yao, Z. W. & Zhang, L. 2006 Equilibrium conformation of polymer chains with noncircular cross section. *Phys. Rev. E* **74**, 032801. (doi:10.1103/PhysRevE.74.032801)
- Zhou, Z. C., Lai, P. Y. & Joós, B. 2005 Elasticity and stability of a helical filament. *Phys. Rev. E* **71**, 052801. (doi:10.1103/PhysRevE.71.052801)